Splats in Splats: Embedding Invisible 3D Watermark within Gaussian Splatting

Yijia Guo [1*]   Wenkai Huang [2,3*]   Yang Li [1]   Gaolei Li [2,3 ✉]   Hang Zhang [5]
Liwen Hu [1]   Jianhua Li [2,3]   Tiejun Huang [1]   Lei Ma [1,4 ✉]

[1] State Key Laboratory of Multimedia Information Processing, School of Computer Science, Peking University

[2] School of Electronic Information and Electrical Engineering, Shanghai Jiao Tong University

[3] Shanghai Key Laboratory of Integrated Administration Technologies for Information Security, Shanghai Jiao Tong University

[4] College of Future Technology, Peking University [5] Cornell University

Abstract

3D Gaussian splatting (3DGS) has demonstrated impressive 3D reconstruction performance with explicit scene representations. Given the widespread application of 3DGS in 3D reconstruction and generation tasks, there is an urgent need to protect the copyright of 3DGS assets. However, existing copyright protection techniques for 3DGS overlook the usability of 3D assets, posing challenges for practical deployment. Here we describe WaterGS, the first 3DGS watermarking framework that embeds 3D content in 3DGS itself without modifying any attributes of the vanilla 3DGS. To achieve this, we take a deep insight into spherical harmonics (SH) and devise an importance-graded SH coefficient encryption strategy to embed the hidden SH coefficients. Furthermore, we employ a convolutional autoencoder to establish a mapping between the original Gaussian primitives' opacity and the hidden Gaussian primitives' opacity. Extensive experiments indicate that WaterGS significantly outperforms existing 3D steganography techniques, with 5.31% higher scene fidelity and $3\times$ faster rendering speed, while ensuring security, robustness, and user experience. Codes and data will be released at our project page.

1. Introduction

Building on the success of utilizing a discrete 3D Gaussian representation for scenes, 3D Gaussian Splatting (3DGS) [18] significantly accelerates the training and rendering speed of radiance fields with explicit scene representations. Given the widespread application of 3DGS in 3D reconstruction and generation tasks [35, 36], the identification and attribution of 3DGS assets are crucial to ensure their

secure use and protect against copyright infringement. Watermarking can play a key role in verifying the provenance of 3DGS assets and preventing both accidental and deliberate misuse. In addition to ensuring security, fidelity, and robustness as observed in traditional digital watermarks, the digital watermarking technique for 3DGS also must fulfill the following two criteria:

a) Protecting the 3DGS asset itself rather than the rendered image. A straightforward approach for 3DGS watermarking is embedding specific information directly into the rendered images from the 3DGS. However, this method solely safeguards the copyright of the rendered images from specific viewpoints instead of the copyright of the 3DGS itself. Malicious users may generate new samples employing different rendering strategies after stealing the core model, circumventing the external watermarking anticipated by the creators.

b) Ensuring the usability of 3DGS assets. Watermarking techniques must not disrupt the user's normal use of 3DGS assets. Digital watermarks for 2D images [2, 34], videos [24, 26] and Neural Radiance Fields (NeRF) [16, 19] have all ensured this aspect. However, existing 3DGS watermarking techniques such as GS-Hider [40] modify the attributes and rendering pipeline of vanilla 3DGS, as shown in Fig. 1. These methods have an immense effect on users' standard utilization since the watermarked 3DGS asset poses challenges for practical deployment in vanilla 3DGS rendering engines and downstream tasks. The fundamental solution is to keep the attributes of vanilla 3DGS. **Is there a solution that can embed watermark in 3DGS itself without modifying any attributes of the vanilla 3DGS?**

To fulfill the above demands, we propose an effective and flexible watermarking framework named **WaterGS**. To the best of our knowledge, WaterGS is the first framework that embeds 3D content into the vanilla 3DGS while fully preserving its attributes. To achieve this, We take a deep insight into spherical harmonics (SH) and devise
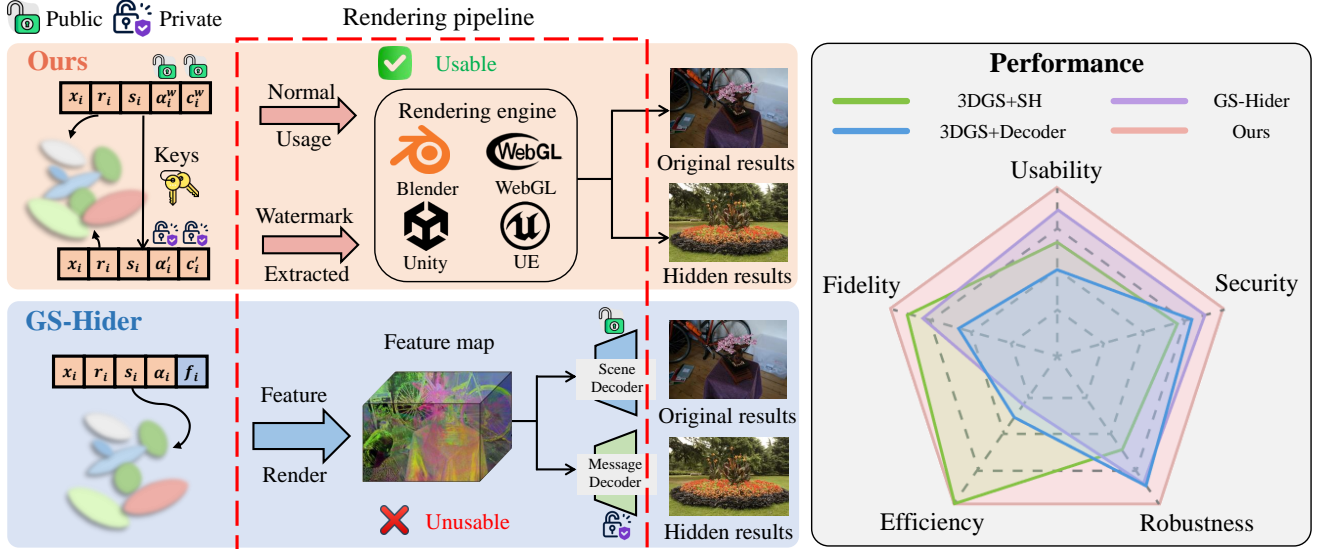
Figure 1. **Left:** GS-Hider and our WaterGS's rendering pipeline. GS-Hider [40] employs a coupled feature field and neural decoders to render the original and hidden scenes simultaneously, affecting user's standard utilization. Our WaterGS keeps the vanilla 3DGS rendering pipeline, preserving user experience. **Right:** Comparison of different 3DGS watermarking methods. Existing works have one or two shortcomings in terms of robustness, fidelity, efficiency, and usability. Our method can maximize the fidelity of the original scene while ensuring the rendering speed and usability of 3DGS, as well as the security of the watermark.

an importance-graded SH coefficient encryption/decryption strategy to embed the hidden SH coefficients. Furthermore, we employ a convolutional autoencoder to establish a mapping between the original Gaussian primitives' opacity and the hidden Gaussian primitives' opacity. WaterGS can also embed other types of digital content, like images, as specific forms of 3D scenes. Our main contributions are as follows:

- We propose WaterGS, the first framework that embeds 3D content in 3DGS itself without modifying any attributes of the vanilla 3DGS.
- Building on a deep insight into the Gaussian primitives' attributes, we devise importance-graded SH coefficient encryption and autoencoder-assisted opacity mapping to preserve the structural integrity of the vanilla 3DGS.
- Extensive experiments indicate that WaterGS achieves state-of-the-art fidelity and efficiency while ensuring security, robustness, and user experience.

2. Related Works

2.1. 3D Gaussian Splatting

Due to the success of utilizing a discrete 3D Gaussian representation of scenes, 3D Gaussian splatting [18] significantly accelerates the training and rendering speed of radiance fields. This breakthrough immediately attracted countless attention. Recently, many researchers have focused on improving the rendering quality [39], effectiveness [8, 9] and the storage [28] of 3DGS, extending it to dynamic 3D scenes [21, 32], large-scale outdoor scenes [23], and high-speed scenes [14, 33, 38], relaxing its restrictions on camera

poses [27] and sharp images [6]. 3DGS is also widely used in the area of inverse rendering [11, 13, 22], 3D generation [35] and 3D editing [7]. Patently, 3DGS is replacing NeRF as the dominant 3D representation and becoming a mainstream 3D asset. Thus, the management of the copyright of 3DGS has been emerging as an urgent problem.

2.2. Digital Watermarking and 3D Steganography

Digital watermarking has continuously evolved from traditional information hiding methods based on domain transformations [3, 15] to watermark encoder and extractor architectures driven by deep learning [1, 41], achieving widespread success in 2D images [2, 34], videos [24, 26], and large-scale generative models [10, 31]. However, 3D steganography techniques place greater emphasis on the unique characteristics of 3D representations. Existing 3D steganography techniques primarily focus on 3D representations like meshes or point clouds, employing domain transformations [17, 20] or homomorphic encryption [30] for information hiding. Yoo *et al.* [37] extracted hidden information from 2D images rendered from different perspectives of a 3D representation, thereby achieving copyright protection.

Recently, steganography techniques on implicit 3D representations like NeRF have gained prominence. Li *et al.* [19] introduced the StegaNeRF framework, embedding secret images into 3D scenes by fine-tuning NeRF's weights, while preserving the original visual quality. CopyNeRF [25] replaced the original color representation in NeRF with a watermarked version, enabling rendered images to con-

tain specific embedded strings and achieved a high bit accuracy. WaterRF [16] introduced a watermarking method for both implicit and explicit NeRF representations which embeds binary messages using discrete wavelet transform, combined with deferred back-propagation, achieving great performance in capacity, invisibility, and robustness. When considering 3DGS, a novel and efficient 3D representation, GS-Hider [40] utilized a scene decoder and a message decoder to disentangle the original scene from the hidden message, allowing for steganography within 3D scenes. However, GS-Hider not only caused a degradation in both rendering speed and visual quality, but also damaged the vanilla 3DGS architecture, resulting in limited effectiveness in practical deployment. So there is an urgent need for 3DGS steganography research that ensures copyright protection while maintaining the efficiency and usability of original 3DGS framework.

3. Preliminary

Different from the widely adopted Neural Radiance Field, 3DGS characterizes Gaussian primitives to represent a 3D scene explicitly. In this representation, every Gaussian primitive G is defined by a full 3D covariance matrix Σ in world space centered at $x \in \mathbb{R}^3$:

$$G(x) = e^{-1/2(x)^T \Sigma^{-1}(x)}. \tag{1}$$

The covariance matrix Σ of a 3D Gaussian primitive can be described as a rotation matrix R and a scale matrix S and independently optimize of both them.

$$\Sigma = RSS^T R^T. \tag{2}$$

Further, we utilize the method of splatting to project our 3D Gaussian primitives to 2D camera planes for rendering:

$$\Sigma' = JW\Sigma W^T J^T. \tag{3}$$

Where J is the Jacobian of the affine approximation of the projective transformation and W is the viewing transformation. Following this, the pixel color is obtained by alpha-blending N sequentially layered 2D Gaussian splats from front to back:

$$C = \sum_{i \in N} c_i \alpha_i \prod_{j=1}^{i-1}(1 - \alpha_j). \tag{4}$$

Where c_i is the color of each point and α_i is given by evaluating a 2D Gaussian with covariance Σ multiplied with a learned per-point opacity.

In summary, each 3D Gaussian primitive is defined by five attributes: $\{x_i, r_i, s_i, \alpha_i, c_i\}$. Specifically, x_i and s_i are represented as 1×3 vectors, while r_i is formatted as a 1×4 vector, and α_i is a scalar value. Notably, c_i is constituted as a $n \times 3$ matrix of Spherical Harmonic (SH) coefficients, which effectively compensates for view-dependent effects.

4. Methodology

4.1. Overview

The overall workflow of the proposed WaterGS is depicted in Fig. 2. Our objective is to seamlessly embed a 3D watermark into 3DGS assets through hidden attributes, while ensuring that the typical usage pipeline for regular users remains unaffected. WaterGS can also embed other types of digital content, like images, as specific forms of 3D scenes. Accordingly, the asset owner can leverage a private key to recover the hidden attributes and extract the 3D watermark, enabling robust verification. To achieve this, we first pre-train hidden SH coefficients and opacity for each 3D Gaussian primitive to align with the watermarking scene. Subsequently, we devise importance-graded SH coefficient encryption/decryption and autoencoder-assisted opacity mapping strategies to effectively accomplish watermark embedding and extraction. With these strategies, WaterGS can not only protect the copyright of 3DGS assets but also maintain the essential attributes of vanilla 3DGS, thereby ensuring its practical usability.

4.2. An Insight in Spherical Harmonics

Any function $F(s)$ is defined on the sphere S can be represented as a set of SH basis functions:

$$F(s) \approx \sum_{l=0}^{n-1} \sum_{m=-l}^{l} f_l^m Y_l^m(s), \tag{5}$$

and the basis functions are defined as:

$$Y_l^m(\theta, \phi) = K_l^m e^{im\phi} P_l^{|m|}, l \in N, m \in (-l, l), \tag{6}$$

where $P_l^{|m|}$ are the associated Legendre polynomials and K_l^m are the normalization constants:

$$K_l^m = \sqrt{\frac{(2l+1)(l-|m|)!}{4\pi(l+|m|)!}}. \tag{7}$$

Low values of l (called the band index) represent low-frequency basis functions over the sphere while high values of l represent high-frequency basis functions. In most cases, higher-frequency reflections occupy only a small proportion of the scene. Consequently, the contribution of higher-order spherical harmonic coefficient is minimal, leading to information redundancy in these higher-order terms, as illustrated in Fig. 3. Embedding watermark information within these terms would pose considerable challenges for detection and would ultimately preserve fidelity. In this paper, we capitalize on this property of spherical harmonics to embed information while simultaneously improving resilience against noise attacks that target spherical harmonics.
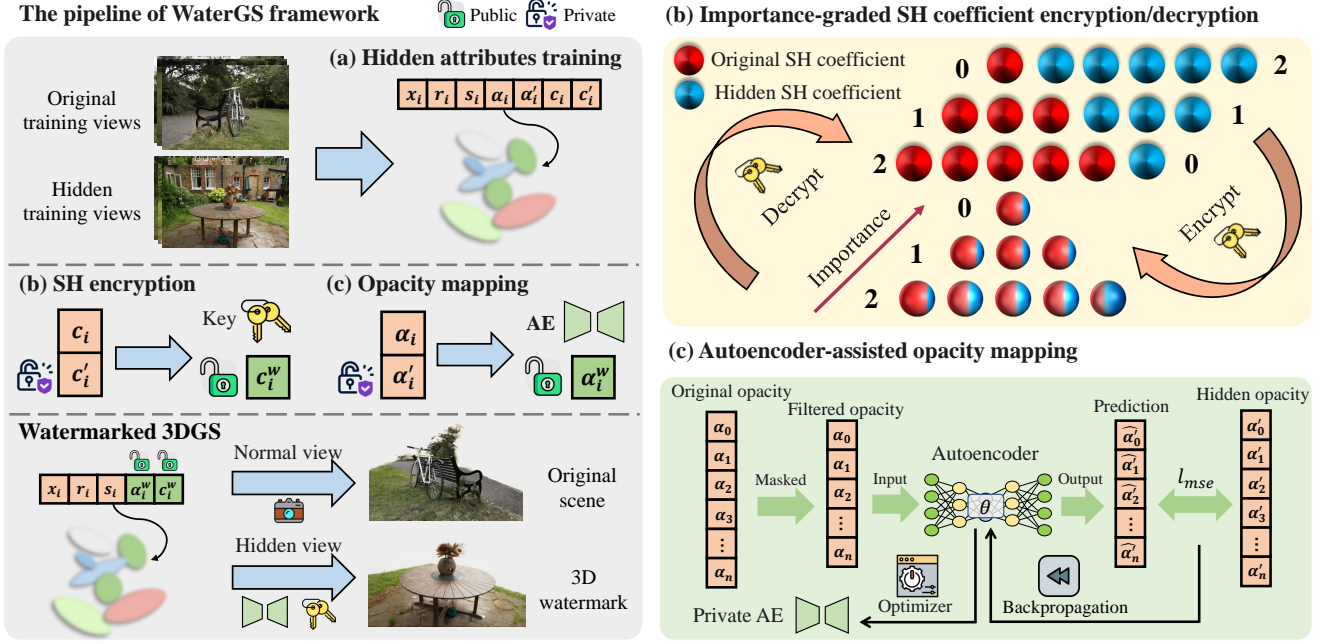
Figure 2. **Overview of the WaterGS Framework**. To ensure a seamless user experience, WaterGS preserves the same attributes as the vanilla 3DGS, while enabling the extraction of embedded 3D watermark information for assets owner. The watermark embedding and extraction process involves three key steps: **a) Hidden attributes training**: We utilize the original and hidden views to train two sets of SH coefficients and opacity, while ensuring that both sets share the same Gaussian primitive locations. **b) Importance-graded SH coefficient encryption/decryption**: We prioritize SH coefficients by significance, embedding more important hidden SH coefficients into higher-order components of the original SH via bit-shifting, aiming to achieve superior rendering fidelity and high robustness against noise attack. **c) Autoencoder-assisted opacity mapping**: We apply a threshold to discard trivial hidden opacities, subsequently employing an convolutional autoencoder to model the transformation from the original opacity to the hidden opacity.

4.3. 3D Watermark Embedding

As illustrated in Fig. 2, we embed the trained hidden SH coefficients and opacities into the original Gaussian primitives. For the SH coefficient encryption, we prioritize SH coefficients by order, embedding the more significant hidden coefficients into the higher-order components of the original SH through bit shifting. For the opacity mapping, we set a threshold to filter out insignificant hidden opacities and utilize an convolutional autoencoder to learn the mapping from the original opacity to the hidden opacity.

4.3.1 Importance-graded SH Coefficient Encryption

For the original SH coefficients $c_i \in \mathbb{R}^{n \times 3}$ and the hidden SH coefficients $c'_i \in \mathbb{R}^{n \times 3}$, let $c_{i,j}$ denote the j-th ($0 \leq j \leq n - 1$) component of c_i. Then, the order of $c_{i,j}$ is $\lfloor \sqrt{j} \rfloor$ according to the definition, where $\lfloor \cdot \rfloor$ denotes the floor function. The lower the order of $c_{i,j}$, the more significant the coefficient is in the Gaussian primitive. Drawing from the insight from Sec. 4.2, we embed more bits of the low-order $c'_{i,j}$ into the higher-order $c_{i,j}$ to achieve higher quality. For computational convenience, we scale these coefficients and represent them in integer form as binary val-

ues of $\{0, 1\}^m$.

Firstly, we nullify the lower bits of $c_{i,j}$ **based on its graded importance**:

$$\tilde{c}_{i,j} = c_{i,j} \ \& \sim ((1 << (k + \lfloor \sqrt{j} \rfloor)) - 1). \quad (8)$$

Where $<<$ denotes left bit shifting operation, $\sim$ operator represents the bitwise NOT operation, and k represents the bit shifting length corresponding to the 0-order coefficient. Subsequently, we shift $c'_{i,j}$ to the corresponding position and **perform an exclusive OR operation with $\tilde{c}_{i,j}$**:

$$c^w_{i,j} = \tilde{c}_{i,j} \oplus (c'_{i,n-1-j} >> (m - (k + \lfloor \sqrt{j} \rfloor))). \quad (9)$$

Where $>>$ denotes right bit shifting operation, m represents the maximum bit length, and $c^w_{i,j}$ denotes the watermarking SH coefficient. The $n - 1 - j$ term indicates that $c'_{i,j}$ has been reversed to match our importance-graded selection. Building on this strategy, we maintain the inherent attributes of original 3DGS, while achieving superior rendering fidelity.

4

Figure 3. Importance of Spherical Harmonics order. We retain the specified order of SH and render the image while setting other orders to zero. Higher-order SH contains only a small amount of High-frequency information.

4.3.2 Autoencoder-assisted Opacity Mapping

To balance the quality of both the original and hidden scenes, we also incorporate hidden opacity attributes and employ a convolutional autoencoder to learn the mapping from original opacity to hidden opacity. Let the original opacity be denoted as $\alpha \in \mathbb{R}^{N \times 1}$ and the hidden opacity attribute as $\alpha' \in \mathbb{R}^{N \times 1}$. We first set a threshold τ to obtain the indices of the more significant hidden opacity values:

$$\mathcal{I} = \{i \mid \alpha'_i > \tau, \ i \in \{1, 2, \dots, N\}\}. \tag{10}$$

Notably, we store the coordinates $x_\mathcal{I}$ of the Gaussian primitives at the indices $\mathcal{I}$, which are then used in the hidden opacity estimation process. Then we denote $\alpha_\mathcal{I}$ and $\alpha'_\mathcal{I}$ as the values of α and α' at $\mathcal{I}$, respectively. Based on the observation that α_i and α'_i exhibit complementary relationships at many positions, we apply an autoencoder to $1 - \alpha_\mathcal{I}$, performing encoding and decoding to obtain $\hat{\alpha}'_\mathcal{I}$. We then utilize the Mean Squared Error (MSE) to train the autoencoder, learning the mapping from $\alpha_\mathcal{I}$ to $\alpha'_\mathcal{I}$:

$$W_p^* = \min_{\mathcal{E},\mathcal{D}} \ell_{mse}(\mathcal{D}(\mathcal{E}(1 - \alpha_\mathcal{I})), \alpha'_\mathcal{I}). \tag{11}$$

Here, $\mathcal{E}$ and $\mathcal{D}$ represent the encoder and decoder, respectively. To ensure real-time rendering, our autoencoder is composed of several simple convolutional and deconvolutional layers. The trained model parameters W_p^* then serve as the private attribute for the owner. Through this strategy, we reduce the storage requirements for the asset owner, while preserving the usability of the watermarked 3DGS.

4.4. 3D Watermark Extraction

In cases of suspected copyright infringement, we can use SH coefficient decryption and opacity estimation to recover the hidden $c'_{i,j}$ and α'_i:

$$c'_{i,j} = c^w_{i,n-1-j} \ \& \ (1 << (k + \lfloor \sqrt{n-1-j} \rfloor)), \tag{12}$$

$$\alpha'_\mathcal{I} = \mathcal{D}_p(\mathcal{E}_p(1 - \alpha_\mathcal{I})). \tag{13}$$

Where $c^w_{i,j}$ is the public watermarked coefficient, and $\mathcal{E}_p$ and $\mathcal{D}_p$ represent the encoder and decoder obtained from

W_p^*, respectively. In practical scenarios, we can choose to retain only the recovered low-order SH coefficients to defend against potential noise attacks. For indices outside of the set $\mathcal{I}$ (i.e., positions from 1 to N not included in $\mathcal{I}$), we set the hidden opacity to zero, as these locations are considered less significant. Finally, we use the recovered attributes $\{x_i, r_i, s_i, \alpha'_i, c'_i\}$ as the hidden 3DGS, which contains the embedded 3D watermark.

5. Experiment

5.1. Implementation Details

Our code is based on 3DGS and we train models for 30000 iterations on NVIDIA A800 GPU with the same optimizer and hyper-parameters as 3DGS. Unless otherwise specified, τ and k in Eq. 10 and Eq. 8 are set to 0.25 and 17.

5.2. Experimental Settings

Datasets: Same as GS-Hider [40], we conduct experiments on 9 original scenes taken from the public Mip-NeRF360 [4] dataset and the correspondence between the hidden and original scene is also the same as GS-Hider. Please refer to our Appendix for more details.

Baselines: we compare our WaterGS with existing 3DGS steganography method GS-Hider [40]. We also use some intuitive approaches with original 3DGS (3DGS+SH and GS+Decoder) as our baselines as [40] did since the available 3DGS watermarking technologies are rare. Meanwhile, we feed the rendering results of the original 3DGS to a U-shaped decoder and constrain it to output hidden scenes according to [19], called 3DGS+StegaNeRF.

Metrics: We evaluate the synthesized novel view in terms of Peak Singal-to-Noise Ratio (PSNR) and Structural Similarity Index Measure (SSIM). Meanwhile, we use rendering FPS to evaluate our efficiency.

5.3. Evaluation of WaterGS

Firstly, we compare our WaterGS with baselines in terms of fidelity, efficiency, robustness, security, and usability.

a) Fidelity: We use Novel View Synthesis (NVS) results to evaluate scene fidelity. As shown in Tab. 1, our WaterGS achieves the best NVS quality on both original and hidden scenes. Fig. 4 shows more visual details which indicate that our waterGS achieves the most appealing visualization results without the artifacts seen in 3DGS+2SH or the erroneous textures and colors observed in StegaNeRF+GS.

b) Efficiency: Tab. 1 also demonstrates that our WaterGS achieves state-of-the-art rendering efficiency, with a rendering speed of over 100 FPS, which is 3x faster than the existing 3DGS watermarking methods using neural networks, such as GS-Hider.

c) Robustness: To evaluate the robustness of 3DGS watermarking method, we degrade the Gaussian primitives using
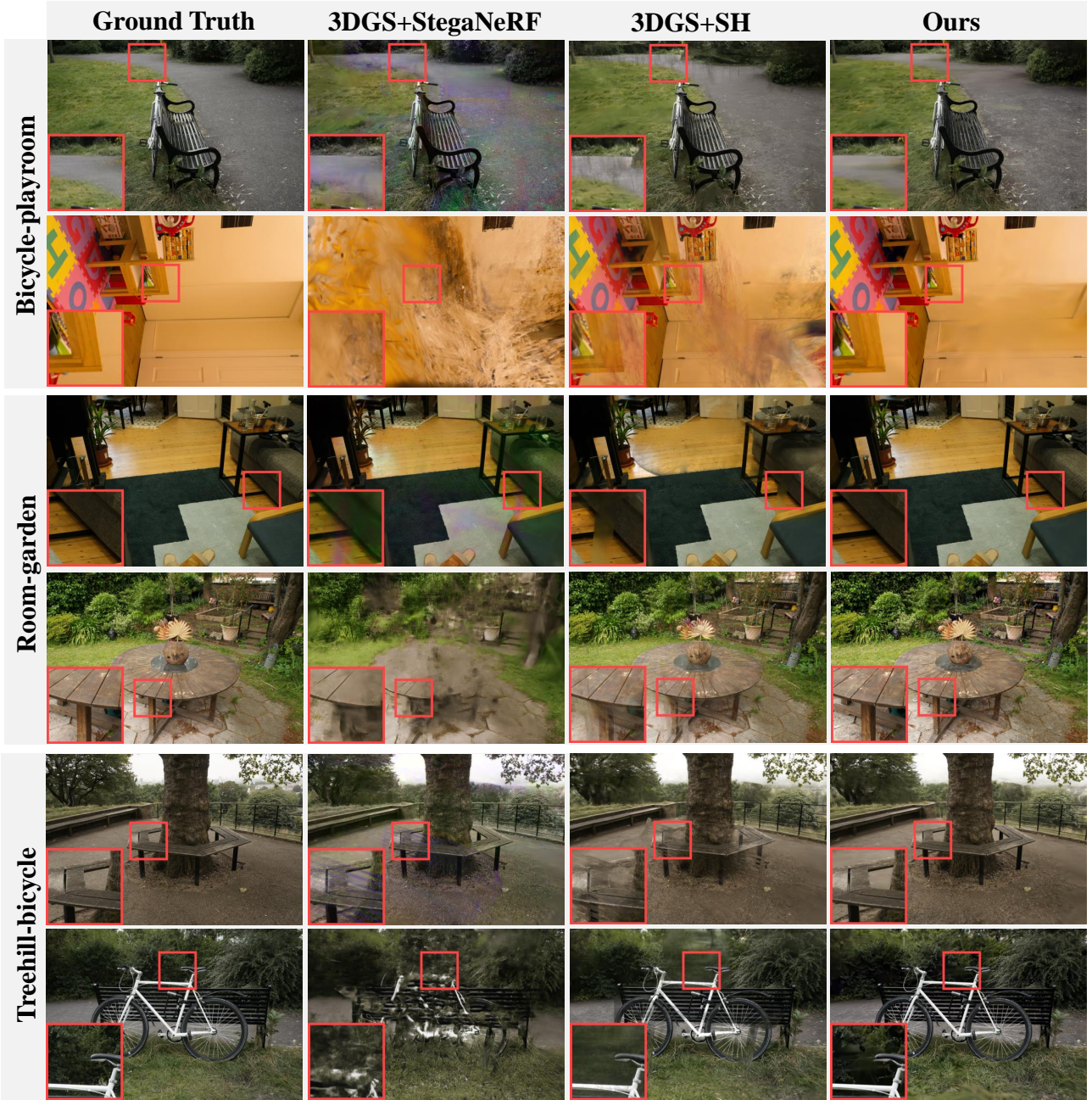
Figure 4. Qualitative comparisons on Mipnerf360 datasets. The first row of each group represents the original scene while the second represents the hidden scene. Our WaterGS achieves sharper results with more consistent structures.

sequential pruning and random pruning methods same as [40]. For sequential pruning, we delete the Gaussian primitives with lower opacity, the results are shown in Tab. 2. For random pruning, we delete the random Gaussian primitives, the results are shown in Tab. 3. Both sequential pruning and random pruning results demonstrate that our WaterGS not only resists the degradation process effectively but also achieves better robustness compared to GS-Hider.

For 25% sequential pruning, our PSNR only decreases by 0.002 while GS-Hider decreases by 0.03. For 25% random pruning, our PSNR only decreases by 0.09 while GS-Hider decreases by 1.26.

d) Security: To evaluate the security of our WaterGS, we employ StegExpose [5], a technique for detecting hidden information in images, to verify whether the rendered images of 3DGS assets contain detectable embedded data. We

Method	Type	SIBR Viewer	Rendering FPS	Bicycle	Flowers	Garden	Stump	Treehill	Room	Counter	Kitchen	Bonsai	Average
3DGS+SH	Scene	✓	100+	23.365	18.998	24.897	22.818	21.479	29.311	26.893	28.150	26.286	24.689
	Message	✓	100+	23.548	25.080	28.450	24.067	20.619	22.231	20.997	22.758	21.340	23.232
3DGS+Decoder	Scene	✓	30+	23.914	19.877	24.284	24.134	21.200	27.502	26.561	26.013	27.674	24.573
	Message	✗	30+	20.611	20.540	25.287	19.933	19.848	21.668	20.670	22.367	20.318	21.249
3DGS+StegaNeRF[19]	Scene	✓	30+	22.789	19.811	23.140	24.260	21.465	28.659	26.400	25.039	25.521	24.120
	Message	✗	30+	15.990	14.753	16.615	16.513	17.543	17.213	16.706	17.534	17.259	16.681
GS-Hider [40]	Scene	✗	30+	24.018	20.109	26.753	24.573	21.503	28.865	27.445	29.447	29.643	25.817
	Message	✗	30+	28.219	26.389	32.348	25.161	20.276	22.885	20.792	26.690	23.846	25.179
Ours	Scene	✓	100+	24.431	20.685	26.831	25.414	22.156	30.930	28.642	30.699	30.953	26.749
	Message	✓	100+	28.988	29.006	29.013	28.811	22.794	23.355	22.514	28.345	25.826	26.517

Table 1. Comparison of the quantitative performance of the original and hidden message scenes. We also report the average rendering speed and the adaptability of SIBR viewer (official rendering engine of 3DGS). **Best** results are marked in red and the second best results are marked in yellow .

Method	GS-Hider [40]		Ours	
Ratio	$PSNR_M \uparrow$	$SSIM_M \uparrow$	$PSNR_M \uparrow$	$SSIM_M \uparrow$
5%	25.179	0.780	26.519	0.797
10%	25.179	0.780	26.518	0.797
15%	25.179	0.780	26.518	0.797
25%	25.167	0.780	26.517	0.797

Table 2. Quantitative comparisons of sequential pruning. Our WaterGS achieves better robustness compared to GS-Hider with lower metrics decline under sequential pruning.

Method	GS-Hider [40]		Ours	
Ratio	$PSNR_M \uparrow$	$SSIM_M \uparrow$	$PSNR_M \uparrow$	$SSIM_M \uparrow$
5%	24.923	0.774	26.415	0.794
10%	24.673	0.767	26.375	0.793
15%	24.371	0.760	26.346	0.793
25%	23.661	0.741	26.320	0.792

Table 3. Quantitative comparisons of random pruning. Our WaterGS achieves better robustness compared to GS-Hider with lower metrics decline under random pruning.

apply StegExpose to the rendered images of different methods to perform anti-forensic detection. The detection set is composed of rendered images from the original scene, mixed with ground truth images at an equal ratio. A higher true positive rate (TPR) and a lower false positive rate (FPR) indicate that the rendered image is more detectable, implying lower security for the watermarking method. Fig. 8 demonstrates that WaterGS exhibits the best security performance among competitive methods, making it highly resistant to detection by StegExpose. For instance, at an FPR of 0.72, WaterGS achieves a TPR of only 0.04, significantly lower than the TPR of 0.16 for both 3DGS+StegaNeRF and 3DGS+SH.

e) Usability: Tab. 1 also demonstrates the adaptability of our WaterGS and baselines to the rendering engine (SIBR Viewer) provided by 3DGS. WaterGS can be directly integrated into the rendering pipeline provided by 3DGS, offer-

ing a seamless user experience that existing approaches are unable to achieve.

In conclusion, our WaterGS achieves both state-of-the-art rendering efficiency and quality while ensuring excellent security, robustness, and user experience.
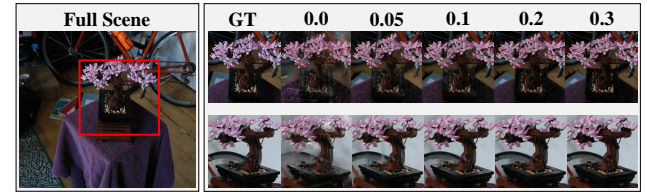

Figure 5. Visualization results of different opacity mask threshold. **Better viewed on screen with zoom in.**

5.4. Ablation Study

a) Opacity mask threshold: We conduct ablations to investigate the effect of different opacity mask thresholds τ. We vary τ in a wide range from 0.0 to 0.3 and plot the average PSNR and SSIM in Fig. 7. Results demonstrate that the opacity mask threshold has a significant influence on rendering quality and WaterGS achieve the best performance when opacity τ is set to 0.25. The visualization results in Fig. 5 further indicate that our opacity mask significantly reduces artifacts and geometric errors, leading to visually
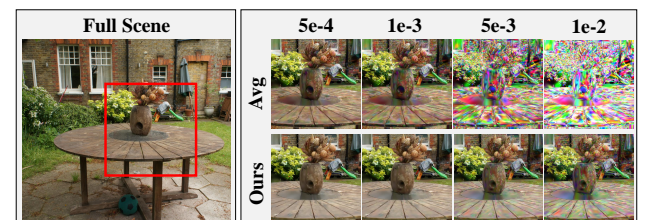

Figure 6. Visualization results under different noise levels. **Better viewed on screen with zoom in.**
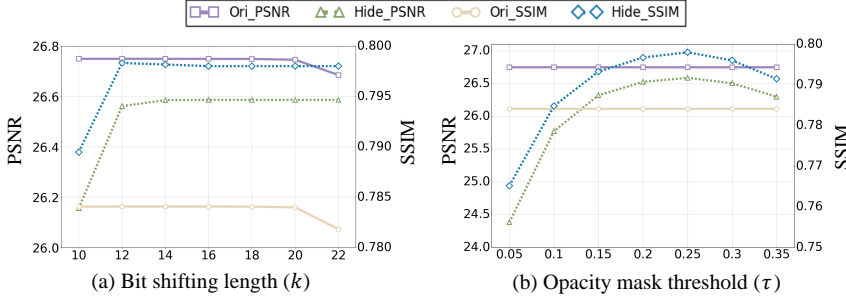
Figure 7. Effect of different shifting lengths k for importance-graded bit encryption/decryption (sub-figure a) and thresholds τ for autoencoder-assisted opacity mapping (sub-figure b) in WaterGS.

Figure 8. ROC curve under StegExpose. For a given false positive rate, a higher true positive rate suggests lower security.

appealing rendering outcomes.

b) Bit shifting length: We vary the bit shifting length k from 10 to 22 and plot the average PSNR and SSIM. The results in Fig. 7 demonstrate that k has minimal impact on rendering results of both original and hidden scene, which further demonstrates the robustness of our method. We provide more comprehensive details in Appendix.

Noise level	0.0005	0.001	0.005	0.01	average
AVG	24.167	21.991	11.442	7.471	16.267
Ours	24.577	24.509	22.797	20.032	22.979

Table 4. Quantitative results of PSNR for rendered hidden images under different noise levels.

c) Importance-graded SH coefficient encryption: We further conduct ablations to illustrate why importance-graded SH coefficient encryption is necessary. We compare the performance of WaterGS with the average encryption (AVG for short) under different levels of Gaussian noise, with noise levels ranging from 0.0005 to 0.01. Quantitative results in Tab. 4 demonstrate that importance-graded encryption offers a significant advantage in noise resistance, which enhances both security and robustness. Figure 6 confirms that as the noise level increases, AVG encryption causes a dramatic degradation in the quality of the recovered hidden scene. In contrast, WaterGS exhibits strong robustness against high-level noise, ensuring successful extraction of the hidden 3D watermark.

5.5. Further Applications

Image Embedding: Our WaterGS can also embed images into the original 3D scene. In fact, this represents a degenerate case of embedding 3D scenes. Similar to GS-Hider, we treat the image embedding task as a scene embedding task with only a single viewpoint. The visualization results in Fig. 9 demonstrate that WaterGS can embed and recover high-quality hidden images from the original scenes with minimal impact on the original scene itself.
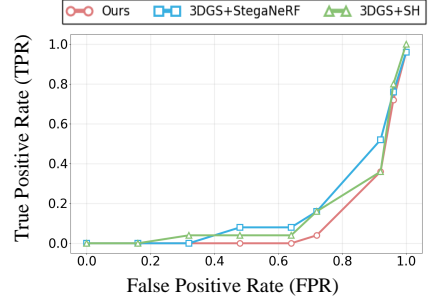
Downstream tasks: Our method provides an excellent

Figure 9. Visualization results of image embedding. We embed CVPR logo (right) into 3D scenes (left).

user experience, demonstrated by its compatibility with all 3DGS rendering pipelines and engines, as well as its seamless integration into downstream tasks utilizing 3DGS. Fig. 10 demonstrates that both original and hidden scenes of our WaterGS can be directly applied to mesh extraction [12] and 3D segmentation [29] with exciting performance. More details are shown in the appendix.
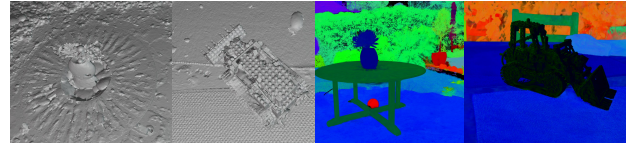

Figure 10. Visualization results of downstream tasks. Our encrypted/decrypted 3DGS scene can be directly used for: **Letf:** Mesh extraction with Sugar (CVPR 24). **Right:** 3D segmentation with Langsplats (CVPR 24 Highlight).

6. Conclusion

We propose WaterGS, an effective and flexible watermarking framework for 3D Gaussian splatting. To the best of our knowledge, WaterGS is the first 3DGS watermarking method that ensures security, fidelity, robustness, and rendering efficiency while maintaining usability and scalability. By carefully designed importance-graded SH coefficient encryption and autoencoder-assisted opacity mapping, WaterGS injects 3D watermarks into the original 3D scenes presented by 3DGS while fully preserving the attributes of the vanilla 3DGS. Extensive experiments indicate that WaterGS achieves state-of-the-art rendering efficiency and fidelity while being well-suited for deployment across diverse applications. This paper offers a promising outlook on provenance verification in 3DGS and calls for more effort on user experience and scalability.

References

[1] Mahdi Ahmadi, Alireza Norouzi, Nader Karimi, Shadrokh Samavi, and Ali Emami. Redmark: Framework for residual diffusion watermarking based on deep networks. *Expert Systems with Applications*, 146:113157, 2020. 2

[2] Shumeet Baluja. Hiding images within images. *IEEE transactions on pattern analysis and machine intelligence*, 42(7): 1685–1697, 2019. 1, 2

[3] Mauro Barni, Franco Bartolini, and Alessandro Piva. Improved wavelet-based watermarking through pixel-wise masking. *IEEE transactions on image processing*, 10(5): 783–791, 2001. 2

[4] Jonathan T. Barron, Ben Mildenhall, Dor Verbin, Pratul P. Srinivasan, and Peter Hedman. Mip-nerf 360: Unbounded anti-aliased neural radiance fields. In *Proceedings of the IEEE/CVF Conference on Computer Vision and Pattern Recognition*, pages 5470–5479, 2022. 5

[5] Benedikt Boehm. Stegexpose-a tool for detecting lsb steganography. *arXiv preprint arXiv:1410.6656*, 2014. 6

[6] Wenbo Chen and Ligang Liu. Deblur-gs: 3d gaussian splatting from camera motion blurred images. *Proceedings of the ACM on Computer Graphics and Interactive Techniques*, 7 (1):1–15, 2024. 2

[7] Yiwen Chen, Zilong Chen, Chi Zhang, Feng Wang, Xiaofeng Yang, Yikai Wang, Zhongang Cai, Lei Yang, Huaping Liu, and Guosheng Lin. Gaussianeditor: Swift and controllable 3d editing with gaussian splatting. *arXiv preprint arXiv:2311.14521*, 2023. 2

[8] Yuedong Chen, Haofei Xu, Chuanxia Zheng, Bohan Zhuang, Marc Pollefeys, Andreas Geiger, Tat-Jen Cham, and Jianfei Cai. Mvsplat: Efficient 3d gaussian splatting from sparse multi-view images. *arXiv preprint arXiv:2403.14627*, 2024. 2

[9] Zhiwen Fan, Wenyan Cong, Kairun Wen, Kevin Wang, Jian Zhang, Xinghao Ding, Danfei Xu, Boris Ivanovic, Marco Pavone, Georgios Pavlakos, et al. Instantsplat: Unbounded sparse-view pose-free gaussian splatting in 40 seconds. *arXiv preprint arXiv:2403.20309*, 2024. 2

[10] Pierre Fernandez, Guillaume Couairon, Hervé Jégou, Matthijs Douze, and Teddy Furon. The stable signature: Rooting watermarks in latent diffusion models. In *Proceedings of the IEEE/CVF International Conference on Computer Vision*, pages 22466–22477, 2023. 2

[11] Jian Gao, Chun Gu, Youtian Lin, Hao Zhu, Xun Cao, Li Zhang, and Yao Yao. Relightable 3d gaussian: Real-time point cloud relighting with brdf decomposition and ray tracing. *arXiv preprint arXiv:2311.16043*, 2023. 2

[12] Antoine Guédon and Vincent Lepetit. Sugar: Surface-aligned gaussian splatting for efficient 3d mesh reconstruction and high-quality mesh rendering. In *Proceedings of the IEEE/CVF Conference on Computer Vision and Pattern Recognition*, pages 5354–5363, 2024. 8

[13] Yijia Guo, Yuanxi Bai, Liwen Hu, Ziyi Guo, Mianzhi Liu, Yu Cai, Tiejun Huang, and Lei Ma. Prtgs: Precomputed radiance transfer of gaussian splats for real-time high-quality relighting. *arXiv preprint arXiv:2408.03538*, 2024. 2

[14] Yijia Guo, Liwen Hu, Lei Ma, and Tiejun Huang. Spikegs: Reconstruct 3d scene via fast-moving bio-inspired sensors. *arXiv preprint arXiv:2407.03771*, 2024. 2

[15] Chiou-Ting Hsu and Ja-Ling Wu. Hidden digital watermarks in images. *IEEE Transactions on image processing*, 8(1):58–68, 1999. 2

[16] Youngdong Jang, Dong In Lee, MinHyuk Jang, Jong Wook Kim, Feng Yang, and Sangpil Kim. Waterf: Robust watermarks in radiance fields for protection of copyrights. In *Proceedings of the IEEE/CVF Conference on Computer Vision and Pattern Recognition*, pages 12087–12097, 2024. 1, 3

[17] Imen Fourati Kallel, Ahmed Grati, and Amina Taktak. 3d data security: Robust 3d mesh watermarking approach for copyright protection. In *Examining Multimedia Forensics and Content Integrity*, pages 1–37. IGI Global, 2023. 2

[18] Bernhard Kerbl, Georgios Kopanas, Thomas Leimkühler, and George Drettakis. 3d gaussian splatting for real-time radiance field rendering. *ACM Transactions on Graphics*, 42 (4):1–14, 2023. 1, 2

[19] Chenxin Li, Brandon Y Feng, Zhiwen Fan, Panwang Pan, and Zhangyang Wang. Steganerf: Embedding invisible information within neural radiance fields. In *Proceedings of the IEEE/CVF International Conference on Computer Vision*, pages 441–453, 2023. 1, 2, 5, 7

[20] De Li, Zhenren Yang, and Xun Jin. Zero watermarking scheme for 3d triangle mesh model based on global and local geometric features. *Multimedia Tools and Applications*, 82 (28):43635–43648, 2023. 2

[21] Deqi Li, Shi-Sheng Huang, Zhiyuan Lu, Xinran Duan, and Hua Huang. St-4dgs: Spatial-temporally consistent 4d gaussian splatting for efficient dynamic scene rendering. In *ACM SIGGRAPH 2024 Conference Papers*, pages 1–11, 2024. 2

[22] Zhihao Liang, Qi Zhang, Ying Feng, Ying Shan, and Kui Jia. Gs-ir: 3d gaussian splatting for inverse rendering. *arXiv preprint arXiv:2311.16473*, 2023. 2

[23] Yang Liu, He Guan, Chuanchen Luo, Lue Fan, Junran Peng, and Zhaoxiang Zhang. Citygaussian: Real-time high-quality large-scale scene rendering with gaussians. *arXiv preprint arXiv:2404.01133*, 2024. 2

[24] Xiyang Luo, Yinxiao Li, Huiwen Chang, Ce Liu, Peyman Milanfar, and Feng Yang. Dvmark: a deep multiscale framework for video watermarking. *IEEE Transactions on Image Processing*, 2023. 1, 2

[25] Ziyuan Luo, Qing Guo, Ka Chun Cheung, Simon See, and Renjie Wan. Copyrnerf: Protecting the copyright of neural radiance fields. In *Proceedings of the IEEE/CVF International Conference on Computer Vision*, pages 22401–22411, 2023. 2

[26] Chong Mou, Youmin Xu, Jiechong Song, Chen Zhao, Bernard Ghanem, and Jian Zhang. Large-capacity and flexible video steganography via invertible neural network. In *Proceedings of the IEEE/CVF Conference on Computer Vision and Pattern Recognition*, pages 22606–22615, 2023. 1, 2

[27] Thomas Müller, Alex Evans, Christoph Schied, and Alexander Keller. Instant neural graphics primitives with a multiresolution hash encoding. *ACM transactions on graphics (TOG)*, 41(4):1–15, 2022. 2

[28] KL Navaneet, Kossar Pourahmadi Meibodi, Soroush Abbasi Koohpayegani, and Hamed Pirsiavash. Compgs: Smaller and faster gaussian splatting with vector quantization. 2

[29] Minghan Qin, Wanhua Li, Jiawei Zhou, Haoqian Wang, and Hanspeter Pfister. Langsplat: 3d language gaussian splatting. In *Proceedings of the IEEE/CVF Conference on Computer Vision and Pattern Recognition*, pages 20051–20060, 2024. 8

[30] Bianca Jansen Van Rensburg, Pauline Puteaux, William Puech, and Jean-Pierre Pedeboy. 3d object watermarking from data hiding in the homomorphic encrypted domain. *ACM Transactions on Multimedia Computing, Communications and Applications*, 19(5s):1–20, 2023. 2

[31] Yuxin Wen, John Kirchenbauer, Jonas Geiping, and Tom Goldstein. Tree-rings watermarks: Invisible fingerprints for diffusion images. *Advances in Neural Information Processing Systems*, 36, 2024. 2

[32] Guanjun Wu, Taoran Yi, Jiemin Fang, Lingxi Xie, Xiaopeng Zhang, Wei Wei, Wenyu Liu, Qi Tian, and Xinggang Wang. 4d gaussian splatting for real-time dynamic scene rendering. *arXiv preprint arXiv:2310.08528*, 2023. 2

[33] Tianyi Xiong, Jiayi Wu, Botao He, Cornelia Fermuller, Yiannis Aloimonos, Heng Huang, and Christopher A Metzler. Event3dgs: Event-based 3d gaussian splatting for fast egomotion. *arXiv preprint arXiv:2406.02972*, 2024. 2

[34] Youmin Xu, Chong Mou, Yujie Hu, Jingfen Xie, and Jian Zhang. Robust invertible image steganography. In *Proceedings of the IEEE/CVF conference on computer vision and pattern recognition*, pages 7875–7884, 2022. 1, 2

[35] Taoran Yi, Jiemin Fang, Guanjun Wu, Lingxi Xie, Xiaopeng Zhang, Wenyu Liu, Qi Tian, and Xinggang Wang. Gaussiandreamer: Fast generation from text to 3d gaussian splatting with point cloud priors. *arXiv preprint arXiv:2310.08529*, 2023. 1, 2

[36] Taoran Yi, Jiemin Fang, Zanwei Zhou, Junjie Wang, Guanjun Wu, Lingxi Xie, Xiaopeng Zhang, Wenyu Liu, Xinggang Wang, and Qi Tian. Gaussiandreamerpro: Text to manipulable 3d gaussians with highly enhanced quality. *arXiv preprint arXiv:2406.18462*, 2024. 1

[37] Innfarn Yoo, Huiwen Chang, Xiyang Luo, Ondrej Stava, Ce Liu, Peyman Milanfar, and Feng Yang. Deep 3d-to-2d watermarking: Embedding messages in 3d meshes and extracting them from 2d renderings. In *Proceedings of the IEEE/CVF Conference on Computer Vision and Pattern Recognition*, pages 10031–10040, 2022. 2

[38] Wangbo Yu, Chaoran Feng, Jiye Tang, Xu Jia, Li Yuan, and Yonghong Tian. Evagaussians: Event stream assisted gaussian splatting from blurry images. *arXiv preprint arXiv:2405.20224*, 2024. 2

[39] Zehao Yu, Anpei Chen, Binbin Huang, Torsten Sattler, and Andreas Geiger. Mip-splatting: Alias-free 3d gaussian splatting. In *Proceedings of the IEEE/CVF Conference on Computer Vision and Pattern Recognition*, pages 19447–19456, 2024. 2

[40] Xuanyu Zhang, Jiarui Meng, Runyi Li, Zhipei Xu, Yongbing Zhang, and Jian Zhang. Gs-hider: Hiding messages into 3d gaussian splatting. *arXiv preprint arXiv:2405.15118*, 2024. 1, 2, 3, 5, 6, 7

[41] Jiren Zhu, Russell Kaplan, Justin Johnson, and Li Fei-Fei. Hidden: Hiding data with deep networks, 2018. 2